Heterocyclic benzothiazole-based liquid crystals: synthesis and mesomorphic properties

Sie-Tiong Ha[ab]; Teck-Ming Koh[a]; Hong-Cheu Lin[c]; Guan-Yeow Yeap[d]; Yip-Foo Win[b]; Siew-Teng Ong[ab]; Yasodha Sivasothy[e]; Lay-Khoon Ong[a]

[a] Faculty of Engineering & Science, Universiti Tunku Abdul Rahman, Jalan Genting Klang, Setapak, Kuala Lumpur, Malaysia [b] Faculty of Science, Engineering & Technology, Universiti Tunku Abdul Rahman, Jalan University, Bandar Barat, Kampar, Perak, Malaysia [c] Department of Materials Science & Engineering, National Chiao Tung Universiti, Hsinchu, Taiwan, ROC [d] Liquid Crystal Research Laboratory, School of Chemical Sciences, University Sains Malaysia, Minden, Penang, Malaysia [e] Chemistry Department, Faculty of Science, Universiti Malaya, Kuala Lumpur, Malaysia

PLEASE SCROLL DOWN FOR ARTICLE

Taylor & Francis
Taylor & Francis Group

Heterocyclic benzothiazole-based liquid crystals: synthesis and mesomorphic properties

Sie-Tiong Ha[a,b]*, Teck-Ming Koh[a], Hong-Cheu Lin[c], Guan-Yeow Yeap[d], Yip-Foo Win[b], Siew-Teng Ong[a,b], Yasodha Sivasothy[e] and Lay-Khoon Ong[a]

[a]*Faculty of Engineering & Science, Universiti Tunku Abdul Rahman, Jalan Genting Klang, Setapak, 53300 Kuala Lumpur, Malaysia;* [b]*Faculty of Science, Engineering & Technology, Universiti Tunku Abdul Rahman, Jalan University, Bandar Barat, 31900 Kampar, Perak, Malaysia;* [c]*Department of Materials Science & Engineering, National Chiao Tung Universiti, 1001 Ta-Hsueh Road, Hsinchu 300, Taiwan, ROC;* [d]*Liquid Crystal Research Laboratory, School of Chemical Sciences, University Sains Malaysia, 11800 Minden, Penang, Malaysia;* [e]*Chemistry Department, Faculty of Science, Universiti Malaya, 50603, Kuala Lumpur, Malaysia*

Two homologous series of 2-(4-alkanoyloxybenzylidenamino)benzothiazoles and 2-(2-hydroxy-4-alkanoyloxy-benzylidenamino)benzothiazoles were synthesised and characterised. Their molecular structures differed wherein the latter comprised a lateral hydroxyl group, unlike the former. Spectroscopic techniques such as FT-IR, ^{1}H & ^{13}C NMR and mass spectrometry together with elemental analysis were employed to elucidate the molecular structures. The transition temperatures and their mesophases were determined by differential scanning calorimetry, optical polarising microscopy and X-ray diffraction techniques. Members with decanoyloxy till hexadecanoloxy chain in the series without the lateral hydroxyl group each exhibited a smectic A phase, while those in the series with the lateral hydroxyl group were non-mesogenic. The mesomorphic properties of the present series were compared with other structurally related series to establish the chemical structure–mesomorphic properties relationship.

Keywords: 2-(4-alkanoyloxybenzylidenamino)benzothiazole; 2-(2-hydroxy-4-alkanoyloxybenzylidenamino)benzo thiazole; Schiff base; smectic A; structure–property relationship

1. Introduction

The mesomorphic behaviour of an organic compound can be varied by modifying its molecular structure including linking, terminal and core groups. Schiff base (or azomethine), a linking group, is usually incorporated into the molecular structure to increase the length and polarisability anisotropy of the molecular core in order to enhance liquid crystal phase stability (*1*). Schiff bases have been studied intensively (*2–5*) since the discovery of 4-methoxybenzylidene-4'-buty-laniline which exhibited a nematic phase at room temperature (*6*).

However, it is commonly believed that molecular order in liquid crystal phases depends largely on the mesogenic core structure: its geometry, polarisability, molecular conformation and length-to-breath ratio as well as the number and position of permanent dipole moments in the core. For this reason, altering the core structure has been regarded as one of the factors that bring significant changes to mesomorphic properties (*1*). Recently, several kinds of heterocyclic rings, such as pyridine (*7*), thiophene (*8*) and 1,3,4-thiadiazole (*9*), have been introduced into the compounds as mesogenic cores. Heterocycles are of great importance as core units in thermotropic liquid crystals owing to their ability to impart lateral and/or longitudinal dipoles combined with

changes in the molecular shape (*10,11*). Furthermore, the incorporation of heteroatoms results in considerable changes in the corresponding liquid crystalline phases and/or in the physical properties of the observed phases, as most of the heteroatoms (S, O, and N) commonly introduced are more polarisable than carbon (*12*).

In addition, heterocyclic rings fused with benzene rings are now becoming popular mesogenic cores to be incorporated into the molecular structure. The meso-morphic properties of heterocyclic fused-ring deriva-tives such as 2,1,3-benzothiadiazole (*13*), benzoxazole (*14*) and 2,1,3-benzoxadiazole (*15*) have been recently studied. The unsaturation and/or the more polarisable nature of the heterocyclic fused-ring systems have greatly affected the mesomorphic properties of cala-mitic molecules (*16*).

Benzothiazole, another kind of heterocyclic fused-ring system, exhibits good hole-transporting proper-ties with a low ionisation potential, making it of poten-tial interest as hole-transporting materials in organic light-emitting devices (OLEDs) (*17*). However, only scant information on the incorporation of benzothia-zole as a core in liquid crystalline compounds (*18–20*) is available. In addition, benzothiazole has also been proved to be a good core in mesogens in our recent study (*21,22*).

Previous study of a series of Schiff base esters has shown that the presence of a lateral hydroxyl group at the *ortho* position led to an increase in the molecular polarisability as well as in the clearing temperature (*23*). A lateral hydroxyl group, on the other hand, can enhance the stability of a molecule through intramolecular hydrogen bonding (*24*). However, the lateral substituents can also disturb the molecular order in liquid crystalline phases or even completely diminish the mesophases (*25*). Therefore, the influence of a lateral hydroxyl group on the mesomorphic properties of benzothiazoles is also one of the interests of the current study.

Herein, we describe the preparation of two homologous series of Schiff base esters with benzothiazole and aromatic cores, 2-(4-alkanoyloxybenzylidenamino) benzothiazoles and 2-(2-hydroxy-4-alkanoyloxybenzylidenamino)benzothiazoles. Fourier transform infrared (FT-IR), ^{1}H & ^{13}C nuclear magnetic resonance (NMR), electron ionization mass spectroscopy (EI-MS) and elemental analysis were employed to elucidate the molecular structure of the title compounds, whereas the liquid crystal behaviours were determined by differential scanning calorimetry (DSC), polarising optical microscopy (POM) and X-ray diffraction (XRD) analysis. In addition, the relationship between the molecular structure and liquid crystal properties is also discussed in this paper.

2.   Experimental

2.1   Characterisation

FT-IR analyses were performed on a Perkin-Elmer System 2000 FT-IR Spectrophotometer. Spectra were obtained by the KBr disc procedure and the range of measurement was from 4000 to 400 cm^{-1}. ^{1}H NMR (400 MHz) and ^{13}C NMR (100 MHz) spectra were recorded in CDCl$_3$ using a JEOL LA-400 MHz NMR spectrometer with TMS as the internal standard. EI-MS (70 eV) were measured with a Mass Spectrometer Finnigan MAT95XL-T at a source temperature of 200°C. Microanalyses were carried out on a Perkin Elmer 2400 LS Series CHNS/O analyser. TLC was carried out on aluminium-backed silica-gel plates (Merck 60 F$_{254}$) and visualised under short-wave ultraviolet light.

Phase-transition temperatures and enthalpy changes were measured using a Differential Scanning Calorimeter Mettler Toledo DSC823^e at heating and cooling rates of 10°C/min and -10°C/min, respectively. A polarising optical microscope (Carl Zeiss) equipped with a Linkam heating stage was used for temperature-dependent studies of the liquid crystal textures. A video camera (Video Master coomo20P) installed on the polarising microscope was coupled to a video

capture card (Video Master coomo600), allowing real-time video capture and image saving. Textures exhibited by the compounds were observed using polarised light with crossed polarisers. Samples were prepared as thin films sandwiched between a glass slide and a cover slip. Phase identification was made by comparing the observed textures with those reported in the literature (*26,27*).

Synchrotron powder XRD measurements were performed at beamline BL17A of the National Synchrotron Radiation Research Center (NSRRC) in Taiwan, where the X-ray wavelength used was 1.32633 Å. XRD data were collected using imaging plates (IP, of an area = 20 × 40 cm^2 and a pixel resolution of 100) curved with a radius equivalent to the sample-to-image plate distance of 280 mm, and the diffraction signals were accumulated for 3 min. The powder samples were packed into a capillary tube and heated by a heat gun, where the temperature controller was programmed by a PC with a proportional–integral–derivative (PID) feedback system. The scattering angle theta was calibrated by a mixture of silver behenate and silicon.

2.2   Synthesis

4-(*N,N*-dimethylamino)pyridine (DMAP) and fatty acids (C$_{n-1}$H$_{2n-1}$COOH where n = 2, 4, 6, 12, 14, 16, 18) were obtained from Merck (Germany). 2-Aminobenzothiazole, 2,4-dihydroxybenzaldehyde, 4-hydroxybenzaldehyde, propanoic acid, pentanoic acid, octanoic acid, decanoic acid and *N,N'*-dicyclohexylcarbodiimide (DCC) were purchased from Acros Organics (USA). All solvents and reagents were purchased commercially and used without any further purification.

The synthetic routes for all the title compounds are depicted in Scheme 1. The synthesis of each compound in both the series was identical.

2.2.1   Synthesis of benzothiazole 1

2-Aminobenzothiazole (40 mmol, 6.01 g) and the appropriate benzaldehyde (40 mmol) were dissolved in 60 ml of ethanol. Two drops of acetic acid were added and the mixture was refluxed for 6 h upon stirring. The mixture was then filtered and the filtrate was left to evaporate to dryness. The yellow solid which was formed was recrystallised with ethanol for further reaction.

2.2.2   Synthesis of benzothiazole 2

Benzothiazole **1** (20 mmol), the appropriate fatty acid (20 mmol) and DMAP (4 mmol) were dissolved in a
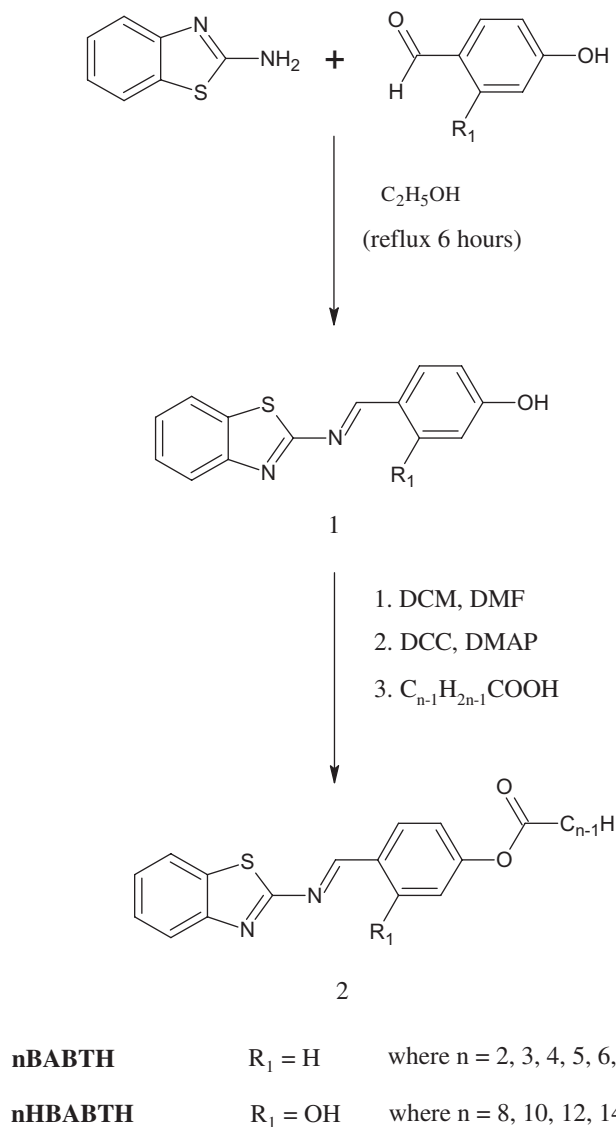
Scheme 1. Synthetic route of *n*BABTH and *n*HBABTH.

50 ml mixture of dichloromethane (DCM) and dimethylformamide (DMF) with the ratio of 4:1 and stirred at 0°C. DCC (20 mmol, 4.13 g) dissolved in 10 ml of dichloromethane was added into the mixture dropwise and continuously stirred for 1 h at 0°C. The mixture was then stirred at room temperature for another 3 h following which it was filtered and the solvent removed by evaporation. The yellow solid which was obtained was recrystallised using ethanol.

The percentage yields and the analytical data of each compound in both the series are tabulated in Tables 1 and 2. The IR, NMR (^{1}H and ^{13}C) and mass spectral data of the representative compounds, **16BABTH** and **16HBABTH**, of both the series are summarised as follows.

16BABTH: IR (KBr) ν_{max} cm^{-1} 3067 (C-H aromatic), 2943, 2891 (C-H aliphatic), 1762 (C=O ester), 1600 (C=N, thiazole). ^{1}H NMR (400 MHz, CDCl$_3$): δ/ppm 0.9 (t, J = 6.6 Hz, 3H, C$\underline{H}_3$-), 1.2–1.4 (m, 24H, CH$_3$-(C$\underline{H}_2$)$_{12}$-CH$_2$-CH$_2$-COO-), 1.8 (quint., J = 7.4 Hz, 2H, -C$\underline{H}_2$-CH$_2$-COO-), 2.6 (t, J = 7.4 Hz, 2H, -C$\underline{H}_2$-COO-), 7.2 (d, J = 8.5 Hz, 2H, Ar-H), 7.3 (t, J = 8.2 Hz, 1H, Ar-H), 7.5 (t, J = 7.2 Hz, 1H, Ar-H), 7.8 (d, J = 8.0 Hz, 1H, Ar-H), 8.0 (d, J = 8.2 Hz, 1H, Ar-H), 8.1 (d, J = 8.5 Hz, 2H, Ar-H), 9.0 (s, 1H, CH=N). ^{13}C NMR (100 MHz, CDCl$_3$): δ/ppm 171.60 (-COO-), 164.71 (C=N), 154.57, 151.65, 134.63, 132.16, 131.44, 126.40, 125.03, 123.03, 122.27, 121.62 for aromatic carbons, 34.35, 31.87, 29.64, 29.62, 29.60, 29.59, 29.54, 29.39, 29.31, 29.19, 29.02, 24.78, 22.64 for methylene carbons [-COO-(C$\underline{H}_2$)$_{14}$-CH$_3$], 14.07

Table 1. Percentage yields and analytical data of *n*BABTH.

| Compound | Yield (%) | Formula | % Found (% Calcd.) | | |
			C	H	N
2BABTH	26	$C_{16}H_{12}N_2O_2S$	64.94 (64.85)	3.97 (4.08)	9.40 (9.45)
3BABTH	30	$C_{17}H_{14}N_2O_2S$	65.72 (65.81)	4.63 (4.52)	9.03 (9.01)
4BABTH	32	$C_{18}H_{16}N_2O_2S$	66.70 (66.64)	4.91 (4.97)	8.53 (8.64)
5BABTH	31	$C_{19}H_{18}N_2O_2S$	67.54 (67.44)	5.33 (5.38)	8.22 (8.30)
6BABTH	29	$C_{20}H_{20}N_2O_2S$	68.12 (68.16)	5.79 (5.72)	7.90 (7.95)
8BABTH	37	$C_{22}H_{24}N_2O_2S$	69.38 (69.44)	6.41 (6.36)	7.33 (7.36)
10BABTH	42	$C_{24}H_{28}N_2O_2S$	70.66 (70.55)	6.83 (6.91)	6.80 (6.86)
12BABTH	44	$C_{26}H_{32}N_2O_2S$	71.59 (71.52)	7.36 (7.39)	6.39 (6.42)
14BABTH	51	$C_{28}H_{36}N_2O_2S$	72.47 (72.38)	7.77 (7.81)	5.94 (6.03)
16BABTH	66	$C_{30}H_{40}N_2O_2S$	73.19 (73.13)	8.19 (8.18)	5.60 (5.69)
18BABTH	73	$C_{32}H_{44}N_2O_2S$	73.71 (73.80)	8.55 (8.52)	5.47 (5.38)

Table 2. Percentage yields and analytical data of *n*HBABTH.

| Compound | Yield (%) | Formula | % Found (% Calcd.) | | |
			C	H	N
8HBABTH	36	$C_{22}H_{24}N_2O_3S$	66.71 (66.64)	6.02 (6.10)	7.05 (7.07)
10HBABTH	44	$C_{24}H_{28}N_2O_3S$	67.81 (67.90)	6.70 (6.65)	6.64 (6.60)
12HBABTH	39	$C_{26}H_{32}N_2O_{\backslash3}S$	69.08 (69.00)	7.10 (7.13)	6.11 (6.19)
14HBABTH	52	$C_{28}H_{36}N_2O_3S$	69.89 (69.97)	7.63 (7.55)	5.87 (5.83)
16HBABTH	64	$C_{30}H_{40}N_2O_3S$	70.72 (70.83)	8.00 (7.93)	5.49 (5.51)

[-COO-$(CH_2)_{14}$-$\underline{C}H_3$]. EI-MS m/z (rel. int. %): 492 (8) $(M)^+$, 254 (100).

16HBABTH: IR (KBr) v_{max} cm^{-1} 3439 (O-H), 3053 (C-H aromatic), 2954, 2894 (C-H aliphatic), 1758 (C=O ester), 1618 (C=N, thiazole). ^{1}H NMR (400 MHz, CDCl$_3$): δ/ppm 0.9 (t, J = 6.0 Hz, 3H, C$\underline{H}_3$-), 1.2–1.4 (m, 24H, CH$_3$-(C$\underline{H}_2$)$_{12}$-CH$_2$-CH$_2$-COO-), 1.8 (quint., J = 7.4 Hz, 2H, -C$\underline{H}_2$-CH$_2$-COO-), 2.6 (t, J = 7.4 Hz, 2H, -C$\underline{H}_2$-COO-), 6.7 (d, J = 8.5 Hz, 1H, Ar-H), 6.8 (s, 1H, Ar-H), 7.4 (d, J = 8.0 Hz, 1H, Ar-H), 7.5 (t, J = 8.5 Hz, 2H, Ar-H), 7.8 (d, J = 8.0 Hz, 1H, Ar-H), 8.0 (d, J = 8.2 Hz, 1H, Ar-H), 9.2 (s, 1H, CH=N), 12.5 (s, 1H, -OH). ^{13}C NMR (100 MHz, CDCl$_3$): δ/ppm 171.38 (-COO-), 168.85 (C=N), 166.35, 163.31, 156.32, 151.43, 135.02, 134.65, 126.71, 126.26, 123.00, 121.72, 116.20, 113.85, 110.70 for aromatic carbons, 34.42, 31.90, 29.65, 29.62, 29.57, 29.42, 29.33, 29.22, 29.04, 24.80, 22.67 for methylene carbons [-COO-($\underline{C}H_2$)$_{14}$-CH$_3$], 14.10 [-COO-(CH$_2$)$_{14}$-$\underline{C}H_3$]. EI-MS m/z (rel. int. %): 508 (12) $(M)^+$, 270 (100).

3. Results and discussion

Structural identification of the title compounds was carried out by employing a combination of elemental analysis and spectroscopic techniques (FT-IR, NMR and EI-MS). The percentages of C, H and N from the elemental analysis conform with the calculated values for compounds *n*BABTH and *n*HBABTH. The prominent molecular ion peaks of **16BABTH** and **16HBABTH** at m/z 492 and 508, respectively, in the mass spectra established a molecular formula of $C_{30}H_{40}N_2O_2S$ and $C_{30}H_{40}N_2O_3S$, supporting the proposed structures.

3.1 FT-IR, ^{1}H NMR and ^{13}C NMR spectral studies

The FT-IR spectra of the title compounds in both the series showed similarities, thus, **16BABTH** was discussed as a representative. From the FT-IR spectrum, the diagnostic absorption band resulting from the C=O stretch of the ester group was present at 1762 cm^{-1} while those of the alkyl groups were observed between 2894 and 2954 cm^{-1}. The relative intensity of the absorption bands of the alkyl groups increased upon ascending the series due to the increasing number of carbons in the alkyl chain. The absorption peak of the azo-methine (C=N) group was overlapping with the absorption band arising from the C=N stretch of

the benzothiazole ring, resulting in a sharp and strong absorption peak at 1600 cm^{-1}.

There was a resemblance between the ^{1}H NMR spectra of **16BABTH** and **16HBABTH** in the region between δ 0.9 and 2.6 ppm. The triplets at δ 0.9 ppm in both the spectra were assigned to the terminal methyl protons. The multiplets between δ 1.2 and 1.4 ppm, the quintet at δ 1.8 ppm and the triplet at δ 2.6 ppm were attributed to the remaining methylene protons [CH$_3$-(C$\underline{H}_2$)$_{14}$-] of the alkanoyloxy chain. The ^{1}H NMR spectra of **16BABTH** and **16HBABTH** confirmed the presence of eight and seven aromatic protons, respectively. The singlet arising from the azomethine proton, was detected at δ 9.0 and 9.2 ppm for **16BABTH** and **16HBABTH**, respectively. However, in the case of **16HBABTH**, an intense singlet at δ 12.5 ppm due to the presence of the lateral hydroxyl group was observed in its spectrum.

In the ^{13}C NMR spectra, the peaks at δ 171.60 and 171.38 ppm were respectively assigned to the carbonyl carbon (-COO-) of **16BABTH** and **16HBABTH** and this was in agreement with that reported in the literature (*22*) while those of the azomethine carbon (CH=N) appeared at 164.71 and 168.85 ppm, respectively. The signals in the region between δ 110.70–166.35 ppm supported the presence of the benzothiazole and aromatic moieties. The carbon resonances between δ 14.07 and 34.35 ppm were indicative of the methylene and methyl carbons of the alkanoyloxy chain. The results as inferred from the IR and NMR spectral data of the title compounds were consistent with the proposed structure.

3.2 Mesomorphic properties of nBABTH and nHBABTH

The transition temperatures during the heating and cooling scans and associated enthalpy changes of **nBABTH** and **nHBABTH** were determined using DSC analysis and are summarised in Tables 3 and 4. The *n*-decanoyloxy up to the *n*-octadecanoyloxy derivatives of **nBABTH** exhibited smectic A phase while **nHBABTH** was a non-mesogenic series. The DSC thermograms of **8BABTH**, **10BABTH** and **12BABTH** during the heating and cooling scans are depicted in Figure 1. Figure 1(a) revealed that **8BABTH** is a non-mesogenic compound since only a crystal–isotropic transition temperature was observed. However, an additional phase transition was detected for **10BABTH** (Figure 1(b)) and **18BABTH** upon cooling from the isotropic liquid. Therefore it is a monotropic liquid crystal whereby the melting points are always equal to or higher than the clearing points, hence enabling it to exhibit supercooling properties (*1*). Conversely, **12BABTH**,

Table 3. Transition temperatures and associated enthalpy changes of **nBABTH** upon heating and cooling.

Compound	Transition temperatures, °C (ΔH, kJmol^{-1})
2BABTH*	Cr 125.5 (31.82) I
3BABTH	Cr 141.1 (12.48) I
	Cr 114.7 (11.73) I
4BABTH	Cr 99.7 (20.70) I
	Cr 63.0 (20.38) I
5BABTH	Cr 83.6 (22.32) I
	Cr 54.2 (22.43) I
6BABTH	Cr 92.0 (23.80) I
	Cr 45.4 (20.36) I
8BABTH	Cr 94.2 (7.74) I
	Cr 82.3 (7.26) I
10BABTH	Cr 88.2 (35.83) I
	Cr 51.5 (26.79) SmA 71.4 (6.34) I
12BABTH	Cr 80.8 (45.07) SmA 85.6 (7.44) I
	Cr 52.7 (37.81) SmA 81.7 (8.17) I
14BABTH	Cr$_1$ 55.7 (3.23) Cr$_2$ 82.3 (38.22) SmA 90.7 (10.32) I
	Cr$_1$ 49.5 (2.36) Cr$_2$ 61.9 (35.18) SmA 87.9 (10.23) I
16BABTH	Cr$_1$ 64.9 (2.21) Cr$_2$ 79.5 (2.61) Cr$_3$ 87.3 (44.24) SmA 92.3 (8.73) I
	Cr$_1$ 57.3 (3.71) Cr$_2$ 67.8 (44.72) SmA 89.1 (9.79) I
18BABTH	Cr$_1$ 69.6 (3.44) Cr$_2$ 91.5 (64.29) I
	Cr$_1$ 63.7 (3.84) Cr$_2$ 75.6 (48.69) SmA 89.4 (10.41) I

The values in *italics* were taken during the cooling cycle.
Cr = Crystal; SmA = Smectic A; I = Isotropic liquid.
*No cooling data due to decomposition.

Table 4. Transition temperatures and associated enthalpy changes of **nHBABTH** upon heating and cooling.

Compound	Transition temperatures, °C (ΔH, kJmol^{-1})
8HBABTH	Cr 124.5 (31.10) I
	Cr 102.0 (30.48) I
10HBABTH	Cr 103.5 (31.02) I
	Cr 92.1 (29.59) I
12HBABTH	Cr 99.9 (40.86) I
	Cr 88.5 (39.40) I
14HBABTH	Cr 103.3 (42.07) I
	Cr 93.2 (39.90) I
16HBABTH	Cr$_1$ 72.2 (9.37) Cr$_2$ 106.9 (52.62) I
	Cr 79.2 (29.21) I

The values in *italics* were taken during the cooling cycle.
Cr = Crystal; I = Isotropic liquid.

14BABTH and **16BABTH** are enantiotropic liquid crystals as the liquid crystal phase was observed during the heating and cooling scans.

Optical photomicrographs of **10BABTH** and **16BABTH** are shown in Figure 2 as the representative illustration. Upon cooling the isotropic liquid of **10BABTH**, the SmA phase emerged as bâtonnet (Figure 2(a)) coalescing to form a focal-conic fan-shaped texture. Upon cooling of **16BABTH**, the co-existence of fan-shaped and homeotropic (dark
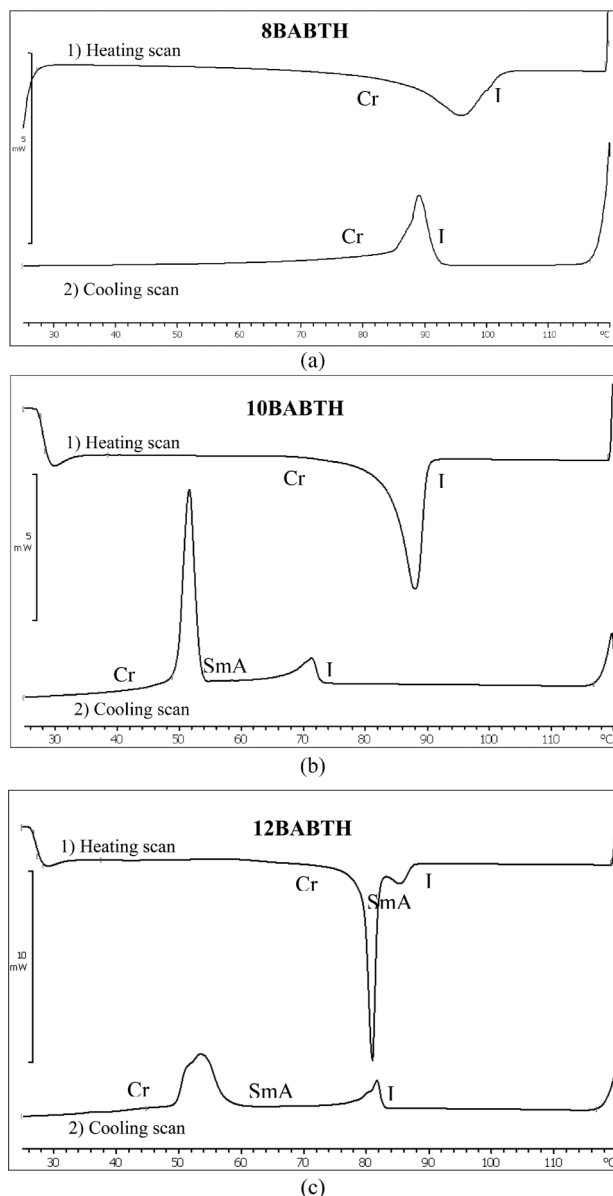
(a)

(b)

(c)

Figure 1. Differential scaning colorimetry thermograms of **8BABTH**, **10BABTH** and **12BABTH** during heating and cooling cycles.

region) textures (Figure 2(b)) were observed. In the homeotropic region, the director of the phase is orthogonal to the layer planes. Consequently, the observed phase was assigned as a SmA phase. All observed liquid crystalline textures are typical according to the literatures (*26,27*).

Figure 3 shows the graph of phase transition temperature versus the number of carbons in the alkanoyloxy chain of **nBABTH**. It is obvious that the short chain derivatives (*n* = 2, 3, 4, 5, 6, 8) were non-mesogens. The liquid crystal phase starts to emerge as a monotropic (metastable) SmA phase beginning with the *n*-decanoyloxy derivative. As
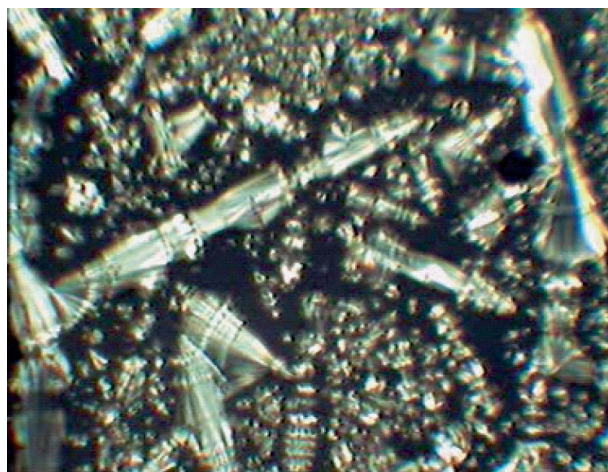
(a)
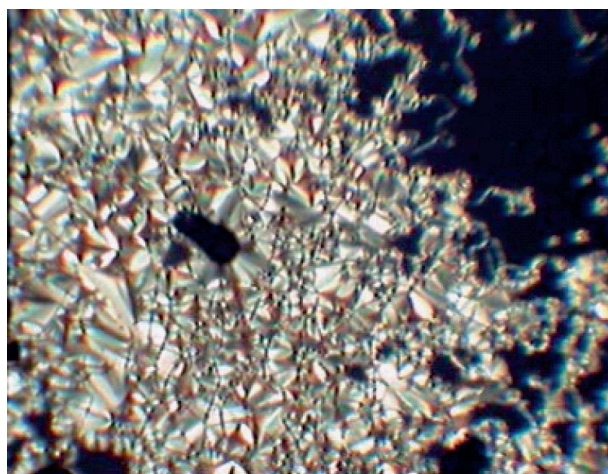
(b)

Figure 2. (a) Optical photomicrograph of **10BABTH** where smectic A phase emerged as bâtonnet upon cooling from isotropic liquid; (b) optical photomicrograph of **16BABTH** exhibiting smectic A phase with fan-shaped and homeotropic (dark area) textures.

the length of the carbon chain increases from the *n*-dodecanoyloxy to the *n*-hexadecanoyloxy derivative, the enantiotropic (stable) SmA phase was observed. The SmA phase range increased from **12BABTH** (4.8°C) to **14BABTH** (8.4°C) and then decreased for **16BABTH** (5.0°C). Upon further increasing the length of the carbon chain, the SmA phase for **18BABTH** turns to a monotropic phase. This phenomenon could have resulted from the flexibility provided by the carbon chain. Generally, high rigidity of a molecule can prevent the formation of a mesophase (*1*). Once the length of the terminal chain is increased, the molecule becomes more flexible hence promoting a monotropic mesophase in a particular compound. If the length of the carbon chain keeps increasing, it may generate an
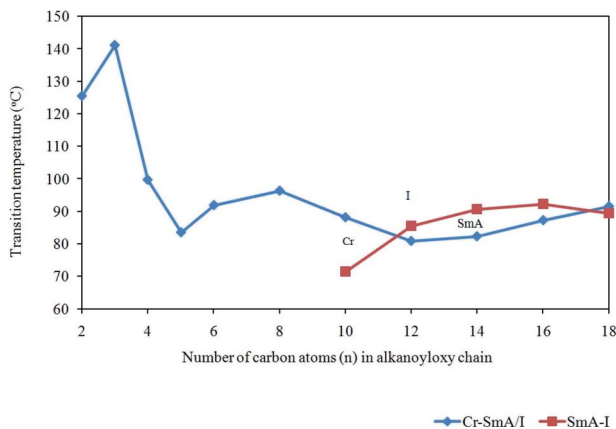
Figure 3. Plot of transition temperatures versus the number of carbons (*n*) in the alkanoyloxy chain of *n*BABTH during heating cycle.

enantiotropic mesophase. However, a continual increase in the length of the carbon chain will depress the stability of the mesophase or even completely diminishing the mesophase formation.

3.3   X-ray diffraction studies

Generally, the types of liquid crystal phases can be preliminarily concluded based on the DSC and POM analysis. In order to further confirm the smectic phase, temperature-dependent XRD analysis was employed whereby the additional information regarding the layered structure was obtained. The XRD pattern of the representative compound **14BABTH** is shown in Figure 4.

In Figure 4, the diffraction pattern showed one sharp peak at a lower region angle and one weak and
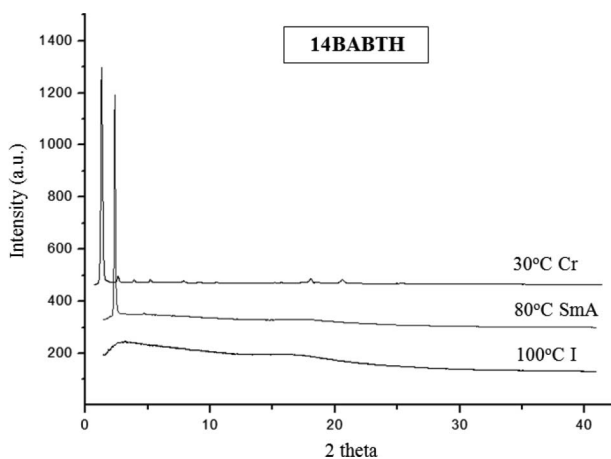

Figure 4. X-ray diffraction patterns of **14BABTH** at different temperatures upon cooling from the isotropic phase.

broad peak at a wider angle. This kind of diffraction pattern is characteristic of a layered structure observed for a smectic phase (*23–25*). The XRD patterns of **14BABTH** at 80°C revealed a sharp diffraction peak at 2.35°, implying the formation of a layered structure. In general, a sharp and strong peak at a low angle ($1° < 2\theta < 6°$) in a small-angle X-ray scattering curve is observed for smectic structures, unlike nematic and cholesteric structures (*28–30*).

The *d*-layer spacing upon cooling **14BABTH** from the isotropic liquid was 35.52 Å whereas the molecular length obtained by MM2 molecular calculation was 31.93 Å. Since the *d/l* ratio was calculated to be 1.11 (*d/ l* ~ 1), the SmA phase for **14BABTH** was suggested to have a monolayer arrangement (*31*).

3.4   Chemical structure–mesomorphic property relationship

The mesomorphic behaviour of an organic compound is dependant on its molecular architecture. Thus, a detailed study of a homologous series may help to derive some general rules on how chemical constitution is able to affect nematogenic and smectogenic compounds, or even the mesophase ranges. In Table 5, the transition temperatures, types of mesophases, mesophase range and molecular structures of *n*BABTH and *n*HBABTH are compared with structurally related compounds **A** (*19*), **B** (*23*) and **C** (*32*).

The difference between the molecular structures of **10BABTH** and compound **A** is in the attachment of the alkoxyl chain ($C_{10}H_{21}O$-) to the benzothiazole core in the latter and the absence of it from the former. While **10BABTH** exhibited a monotropic (metastable) SmA phase, compound **A** exhibited enantiotropic SmC and nematic phases. The presence of the terminal alkoxyl chains identical in length at both sides of the mesogenic core of compound **A** helped to generate the more stable (enantiotropic) smectic phase. Unlike **10BABTH** which exhibited a non-tilted (SmA) mesophase, compound **A** exhibited a tilted (SmC) mesophase. This could have resulted from the influence of the alkoxyl chain at the sixth position of the benzothiazole moiety. An ethoxyl or a longer alkoxyl chain tends to favour the intermolecular interactions giving rise to a tilted arrangement of the molecules in the smectic layers (*21*).
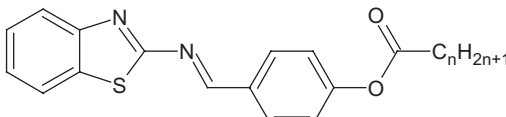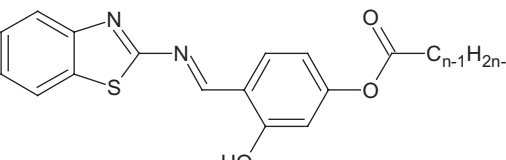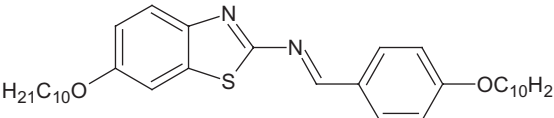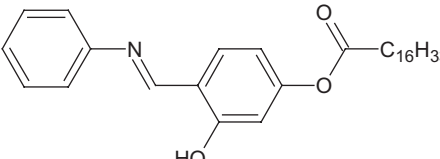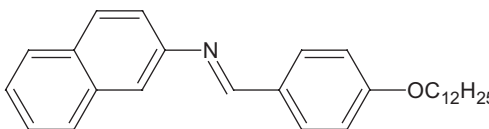
16HBABTH is a non-mesogenic compound whereas a SmA phase was observed for compound **B**. Both structures differ only in the mesogenic core whereby **16HBABTH** comprised a benzothiazole ring while compound **B** a benzene ring. The fused-ring system of benzothiazole tends to increase the molecular breadth, resulting in the thickening effect which disrupts the liquid crystalline packing (*33*).

924   *S.T. Ha* et al

In order to reveal the effect of the lateral hydroxyl group on mesomorphic properties, the molecular structures and phase behaviours of both the title compounds were compared. ***n*BABTH** (where *n* = 10–18) without the lateral hydroxyl group, exhibited a SmA phase whereas ***n*HBABTH** with the lateral hydroxyl group is a non-mesogenic series. Generally, lateral substituents will disturb the molecular packing, hence reducing the mesophase stability (*1*). However, in this case, the absence of the mesophase in ***n*HBABTH** can be explained by the presence of the lateral hydroxyl group that reduces the molecular length-to-breadth ratio, therefore diminishing the mesophase in ***n*HBABTH**. A similar structure–properties relationship can be inferred by comparing the molecular structure of **12HBABTH** and compound **C**. The compound without a lateral hydroxyl group (compound **C**) is still able to exhibit mesophases despite having a broader naphthalene molecule. However, the presence of the lateral hydroxyl group in ***n*HBABTH** disturbed the molecular ordering required to generate a liquid crystal phase.

Table 5. Transition temperatures, mesophase range and molecular structures of ***n*BABTH**, ***n*HBABTH**, A, B and C.

Compound	Transition temperatures (°C)	Mesophase range (°C)	
		Sm	N
10BABTH	Cr 88.2 (SmA 71.4)* I	-	-
12HBABTH	Cr 99.9 I	-	-
16HBABTH	Cr 106.9 I	-	-
A	Cr 81.3 SmC 121.6 N 122.7 I	40.3	1.1
B	Cr 68 SmA 86 I	18.0	-
C	Cr 92 (SmA 76 N 79)* I	-	-

Note: ( )* Monotropic value

4. Conclusions

In this paper, we have described the synthesis and mesomorphic behaviour of two homologous series of 2-(4-alkanoyloxybenzylidenamino)benzothiazoles and 2-(2-hydroxy-4-alkanoyloxybenzylidenamino)-benzothiazoles. The *n*-decanoyloxy to the *n*-octadeca-noyloxy derivatives of **nBABTH** exhibited a SmA phase. **nHBABTH** is a non-mesogenic series due to the presence of the lateral hydroxyl group. The study also revealed that the mesophase range was greatly affected by the length of the terminal chain. In addition, the terminal group at the lateral position was also found to influence the molecular tilting.

References

(1) P.J. Collings; M. Hird. *Introduction to Liquid Crystals: Chemistry and Physics*, Taylor & Francis Ltd.: UK, 1998.

(2) (a) Yeap, G.Y.; Ooi, W.S.; Nakamura, Y.; Cheng, Z. *Mol. Cryst. Liq. Cryst.* **2002**, *381*, 169–178. (b) Yeap, G.Y.; Ha, S.T.; Lim, P.L.; Boey, P.L.; Ito, M.M.; Sanehisa, S.; Youhei, Y. *Liq. Cryst.*, **2006**, *33*, 205–211.

(3) So, B.K.; Kim, W.J.; Lee, S.M.; Jang, M.C.; Song, H.H.; Park, J.H *Dyes Pigments* **2007**, *75*, 619–623.

(4) Godzwon, J.; Sienkowska, M.J.; Galewski, Z. *J. Mol. Struc.* **2007**, *884–885*, 259–267.

(5) (a) Ha, S.T.; Ong, L.K.; Ong, S.T; Yeap, G.Y.; Wong, J.P.W.; Koh, T.M.; Lin, H.C. *Chin. Chem. Lett.* **2009**, *20*, 767–770. (b) Ha, S.T.; Ong, L.K.; Wong, J.P.W.; Yeap, G.Y.; Lin, H.C.; Ong, S.T.; Koh, T.M. *Phase Transitions*, **2009**, *82*, 387–397.

(6) Kelker, H.; Scheurle, B. *Angew. Chem. Int. Edn.*, **1969**, *81*, 903–904.

(7) Torralba, M.C.; Huck, D.M.; Nguyen, H.L.; Horton, P.N.; Donnio, B.; Hursthouse, M.N.; Bruce, D.W. *Liq, Cryst.* **2006**, *33*, 399–407.

(8) Eichhorn, S.H.; Paraskos, A.J.; Kishikawa, K.; Swager, T.M. *J. Am. Chem. Soc.* **2002**, *124*, 12742–12751.

(9) Campbell, N.L.; Duffy, W.L.; Thomas, G.I.; Wild, J.H.; Kelly, S.M.; Bartle, K.; O'Neill, M.; Minter, V.; Tuffin, R.P. *J. Mater. Chem.* **2002**, *12*, 2706–2721.

(10) Matharu, A.S.; Chambers-Asman, D. *Liq. Cryst.* **2007**, *34*, 1317–1336.

(11) Gallardo, H.; Magnago, R.F.; Bortoluzzi, A.J. *Liq Cryst.* **2001**, *28*, 1343–1352.

(12) Lai, C.K.; Ke, Y.; Chien-Shen, J.S.; Li, W. *Liq Cryst.* **2002**, *29*, 915–920.

(13) Vieira, A.A.; Cristiano, R.; Bortoluzzi, A.J.; Garllardo, H. *J. Mol. Struc.* **2007**, *875*, 364–371.

(14) Wang, C.S.; Wang, I.W.; Cheng, K.L.; Lai, C.K. *Tetrahedron*, **2006**, *62*, 9383–9392.

(15) Aldred, M.P.; Vlachos, P.; Dong, D.; Kitney, S.P.; Tsoi, W.C.; O'Neill, M.; Kelly, S.M. *Liq. Cryst*. **2005**, *32*, 951–965.

(16) Lai, L.L.; Wang, C.H.; Hsien, W.P.; Lin, H.C. *Mol. Cryst. Liq. Cryst*. **1996**, *287*, 177–181.

(17) (a) Funahashi, M.; Hanna, J.I. *Jpn J. Appl. Phys.* **1996**, *35*, L703–L705.(b) Funahashi, M.; Hanna, J.I. *Phys. Rev. Lett.* **1997,** *78*, 2184–2187.(c) Funahashi, M., Hanna, J.I. *Mol. Cryst. Liq. Cryst.* **1997,** *304*, 429–434.

(18) Pavluchenko, A.I.; Smirnova, N.I.; Titov, V.V.; Kovahev, E.I.; Djumaev, K.M. *Mol. Cryst. Liq. Cryst.* **1976**, *37*, 35–46.

(19) Belmar, J.; Parra, M.; Zuniga, C.; Perez, C.; Munoz, C. *Liq. Cryst.* **1999**, 26, 389–396.

(20) Prajapati, A.K.; Bonde, N.L. *J. Chem. Sci.* **2006**, *118*, 203–210.

(21) Ha, S.T.; Koh, T.M.; Yeap, G.Y.; Lin, H.C.; Boey, P.L.; Win, Y.F.; Ong, S.T.; Ong, L.K. *Mol. Cryst. Liq, Cryst.* **2009**, in press.

(22) Ha, S.T.; Koh, T.M.; Yeap, G.Y.; Lin, H.C.; Beh, J.K.; Win, Y.F.; Boey, P.L. *Chin. Chem. Lett.* **2009**, *20*, 1081–1084.

(23) Yeap, G.Y.; Ha, S.T.; Lim, P.L.; Boey, P.L.; Mahmood. W.A.K. *Mol. Cryst. Liq. Cryst.* **2004**, *423*, 73–84.

(24) Hallsby, A.; Nilsson, M.; Otterholm, B. *Mol. Cryst. Liq. Cryst.* **1982**, *82*, 61–68.

(25) Berdague, P.; Bayle, J.P.; Ho, M.S.; Fung, B.M. *Liq. Cryst.* **1993**, *14*, 667.

(26) Demus, D.; Richter, L. *Textures of Liquid Crystals*, Verlag Chemie: New York, 1978.

(27) Dierking, I. *Textures of Liquid Crystals*, Wiley-VCH: Weinheim, 2003.

(28) Wang, Y.; Zhang, B.Y.; He, X.Z.; Wang, J.W. *Colloid Polym. Sci.* **2007**, *285*, 1077–1084.

(29) Meng, F.B.; Gao, Y.M.; Lian, J.; Zhang, B.Y.; Zhang, F.Z. *Colloid Polym. Sci.* **2008**, *286*, 873–879.

(30) Xiao, W.; Zhang, B.; Cong, Y. *Colloid Polym. Sci.* **2008**, *286*, 267–274.

(31) Liao, C.C.; Wang, C.S.; Sheu, H.S.; Lai, C.K. *Tetrahedron*, **2008**, *64*, 7977–7985.

(32) Vora, R.A.; Prajapati, A.K. *Liq Cryst*. **1998**, *25*, 567–572.

(33) Kumar, S. *Liquid Crystals: Experimental Study of Physical Properties and Phase Transitions*, Cambridge University Press: UK, 2001.